Catalysis Today 246 (2015) 108–115

Contents lists available at ScienceDirect

Catalysis Today

journal homepage: www.elsevier.com/locate/cattod

Pd–Cu interaction in Pd/Cu-MCM-41 catalysts: Effect of silica source and metal content

Patricia Benito[a], Manuel Gregori[a,b], Sara Andreoli[a], Giuseppe Fornasari[a], Francesca Ospitali[a], Stefano Millefanti[b], Maria Sol Avila[c], Teresita F. Garetto[c], Stefania Albonetti[a,*]

[a] Dipartimento di Chimica Industriale "Toso Montanari", Università di Bologna, Viale Risorgimento 4, 40136 Bologna, Italy
[b] Solvay Specialty Polymers SpA, R&D Centre, Bollate, MI 20021, Italy
[c] Catalysis Science and Engineering Research Group (GICIC), INCAPE (UNL-CONICET), Santiago del Estero 2654, 3000 Santa Fe, Argentina

ARTICLE INFO

Article history:
Received 30 April 2014
Received in revised form 28 July 2014
Accepted 20 August 2014
Available online 22 September 2014

Keywords:
Palladium
Copper
MCM-41
Silicate
TEOS
Hydrodechlorination

ABSTRACT

Pd/Cu-MCM-41 catalysts for the hydrodechlorination of $CF_3OCFClCF_2Cl$ to $CF_3OCF{=}CF_2$ were prepared. Palladium- and copper-containing samples (Pd/Cu = 1 molar ratio) were synthesized by adding Pd^{2+} and Cu^{2+} during the formation of MCM-41, and then the slurries were aged by microwave-hydrothermal treatment. The effect of the silica source (silicates or TEOS) and total metal loading (2.4 and 4.0 wt.%) on the chemical–physical properties and catalytic performances was studied. Bimetallic silicate-derived samples show features similar to those of the pristine MCM-41, regardless of the total metal content. Conversely, the long-range order of the mesoporous structure decreases for TEOS-derived catalysts, and large metal contents seem to alter the structure for these materials.

During template removal by thermal treatment, palladium and copper are on the surface of MCM-41 particles, forming $Pd_{1-x}Cu_xO$ solid solutions whose composition is silica source-dependent. The amount of copper in $Pd_{1-x}Cu_xO$ is greater for TEOS-derived samples.

After reduction, both Pd- and Cu-enriched alloys were found by XRD in silicate-derived samples, while XPS measurements indicated that the surface of the catalyst is enriched with copper. XRD and XPS analyses on TEOS samples indicated that the surface Cu/Pd ratio is closer to 1, and fcc PdCu alloys with a high copper content were identified. The composition of metallic particles modifies the selectivity, TEOS-derived catalysts being more selective to the target $CF_3OCF{=}CF_2$.

1. Introduction

$CF_3OCF{=}CF_2$, perfluorovinylether, is currently produced by a commercial process based on dechlorination with Zn [1,2]. This process produces large amounts of $ZnCl_2$, a salt that must be disposed of after the proper work-up. Catalytic hydrogen-assisted gas-phase dechlorination of $CF_3OCFClCF_2Cl$ over metal-supported catalysts may lead to a new sustainable process [3]. Bimetallic Pd/Cu catalysts on active carbon are promising catalysts for this process [4]. Nevertheless, the microporous texture of the support can significantly limit possible applications of the catalytic system because of the reduced mass transfer. Supports with larger pores will overcome the drawbacks. In particular, MCM-41 silicate mesoporous materials with large specific surface area and appreciable resistance to acids [5] are promising alternatives [6,7].

Bimetallic Pd/Cu catalysts are used in hydrodechlorination reactions [8–14] since the combination of both metals gives rise to catalysts capable of anchoring chlorinated reagents with a tailored hydrogenating activity. Hydrodechlorinating performances are strongly related to the Pd–Cu interaction and the size of metallic particles, both features being determined by synthesis and activation procedures [8,10,13]. Thermodynamically stable PdCu alloy crystalline structures depend on the atomic percentage of Pd and Cu and the temperature [15,16]. However, the actual distribution of Pd and Cu on the catalysts is controlled by the synthesis [13,17–20], reduction treatments, and particle sizes [10,20–24]. In impregnated catalysts, the type of salts used and the order of impregnation determine the interaction between Pd and Cu [13,17–20]. Moreover,

* Corresponding author at: Dip. Chimica Industriale "Toso Montanari", Viale Risorgimento 4, 40136 Bologna, BO, Italy. Tel. +39 051 2093681; fax: +39 051 2093679.
E-mail address: stefania.albonetti@unibo.it (S. Albonetti).

http://dx.doi.org/10.1016/j.cattod.2014.08.027
0920-5861/

the Pd/Cu ratio governs the effect of the reduction temperature on the nature of the surfaces exposed by Pd and Cu and the sintering processes [25].

When dealing with MCM-41 materials containing Cu and Pd, the main drawback to be avoided is the segregation of large Cu [26–32] and Pd [33–39] oxide or metallic particles during the catalyst preparation, which is well-known to be dependent on the incorporation method. In bimetallic Pd/Cu-MCM-41 catalysts, we observed that the nature and size of active species depend on the synthesis procedure, namely co-impregnation of $PdCl_2$ and $CuCl_2$ and addition of Pd and Cu during the MCM-41 synthesis as cations or as preformed nanoparticles [6,7]. Moreover, the nature of the silica source (sodium silicate or TEOS) changes the properties of impregnated catalysts [6]. The formation of bimetallic Pd/Cu particles with controlled composition and size is the key aspect in achieving high yields in the hydrodechlorination, thus the synthetic procedure of Pd/Cu-MCM-41 materials should be optimized further. In this work, we gained insight into the effect of the silica source (silicates and TEOS) and metal loading (2.4 and 4.0 wt.%) on the chemical–physical properties and performances of Pd/Cu-MCM-41 catalysts prepared by adding the active species during the MCM-41 synthesis. For comparison purposes, pure MCM-41 supports and monometallic Pd- and Cu-MCM-41 samples prepared with silicate and TEOS were studied.

2. Experimental

2.1. Catalyst preparation

Pure MCM-41 supports were synthesized following the procedures reported by Beck [40] and Cassiers [41] using sodium silicate and TEOS, respectively, as the silica source. Cetyltrimethylammonium bromide (CTAB) was used as the structure-directing. The compositions of the gels were: 1.0 SiO_2:0.55 CTAB:0.14 H_2SO_4:73 H_2O and 1.0 SiO_2:0.25 CTABr:0.20 TMAOH:35 H_2O for silicate-derived and TEOS-derived synthesis. Slurries were hydrothermally treated in a Milestone StartSYNTH microwave oven for 7 h at 125 °C, then filtered, washed, and dried. The template was removed at 540 °C for 6 h in static air. More details about the syntheses can be found elsewhere [6]. Supports were named sil or TEOS.

Pd and Cu were incorporated during the course of the MCM-41 synthesis by adding an acidic $PdCl_2$ and $CuCl_2$ aqueous solution (Pd/Cu = 1/1 molar ratio, pH = 1) to the template solution. The pH of the final mixture was 6.2. After this, syntheses proceeded as for pristine MCM-41. Slurries were microwave-hydrothermally treated as for the pure MCM-41. Two different total metal loadings were used: 2.4 wt.% and 4.0 wt.%. Monometallic catalysts were also prepared with a Pd and Cu loading of 2.4 and 1.5 wt.%, respectively. The $CuCl_2$ solution was not acidified for the preparation of the monometallic catalyst. Catalysts were labeled *x*Pd-sil, *x*Pd-TEOS, *x*Cu-sil, *x*Cu-TEOS, *x*PdCu-sil, and *x*PdCu-TEOS, where *x* denoted the metal loading, i.e. 2.4PdCu-sil.

2.2. Characterization techniques

Small-angle XRD measurements were carried out in a Philips PW1710 diffractometer with a Bragg/Brentano geometry and equipped with a proportional detector, using Ni-filtered Cu Kα radiation (λ = 1.5418 Å). For all catalysts, the diffraction pattern in the 1.6–15°2θ range was collected with a step size of 0.1° and time per step of 10 s. Wide-angle diffractograms were collected over the 31–45 and 37–52°2θ ranges, 0.08° step size, and 500 s counting time in a PANalytical X'Pert diffractometer equipped with a copper anode and a fast X'Celerator detector. HRTEM images were acquired via a TEM/STEM FEI Tecnai F20 working at 200 kV. Samples were prepared by dispersion of the powder in ethanol and deposition on a holey-carbon film supported with a titanium grid.

N_2 adsorption/desorption isotherms at −196 °C were performed in a Micromeritics ASAP 2020 instrument. Samples were previously outgassed for 30 min at 150 °C and 4 Pa, then heated for 120 min at 350 °C. Specific surface area values were obtained by the multi-point BET equation in the 0.05–0.2 p/p^0 range. The pore size distribution was calculated using the NLDFT-statistic method.

Temperature programmed reduction (TPR) analyses were carried out in a Thermo Scientific TPDRO 1100 working with a 5% H_2/Ar reduction mixture. Pelletized catalysts (60–80 mesh) were heated up to 550 °C (rate: 10 °C min^{-1}) and kept at this temperature for 30 min.

X-ray photoelectron spectroscopy measurements (XPS) were performed using a multitechnique system SPECS 150 equipped with a dual Mg/Al X-ray source and a hemispherical PHOIBOS 150 analyzer operating in the fixed analyzer transmission (FAT) mode. Spectra were obtained using a monochromatic Al Kα radiation ($h\nu$ = 1486.6 eV) operated at 200 W and 12 kV. The pass energy for the element scan was 30 eV, with a pressure in the analyzing chamber lower than $5{\cdot}10^{-7}$ Pa. Spectral regions corresponding to C 1s, O 1s, Cu 2p, Pd 3d, and Si 2p core levels were analyzed. Casa XPS software (Casa Software Ltd., UK) was used for data treatment. Spectra were corrected by referencing the XPS C 1s binding energy (284.6 eV) [42]. Before XPS analyses, samples reduced under the same conditions as for catalytic tests were refreshed under a 5% H_2/Ar mixture at 330 °C in the pre-treatment chamber.

DRIFTS experiments were carried out in a Shimadzu IRPrestige-21 spectrophotometer, equipped with an in situ high-temperature/high pressure SpectraTech cell and a liquid nitrogen-cooled MCT detector. The sample holder, a ceramic crucible containing a heating resistor and a thermocouple, was placed inside a dome with CaF_2 windows. The spectral resolution was 4 cm^{-1}, and 40 scans were added. Gas flow rates were 60 mL/min. Reduced samples (under the same conditions as for catalytic tests) were treated in H_2 at 330 °C for 15 min, then in Ar for 10 min at 300 °C, and lastly cooled down in Ar to 30 °C. Background spectra of the samples in Ar were taken from 200 °C to 30 °C, at 50 °C intervals. A flow of 5% CO/He was introduced at 30 °C and the sample spectrum was collected. Then the CO was removed by an Ar flow and the sample temperature was raised from 30 °C to 200 °C, at 50 °C intervals, for collecting the respective DRIFT spectra. The results presented herein are difference spectra, where the background spectra of the sample in Ar served as the reference.

2.3. Catalytic tests

Catalytic tests were carried out with pelletized (60–80 mesh) samples reduced ex situ with a pure H_2 flow at 330 °C for 1 h [6,7]. Once loaded into the reactor, catalysts were treated in a N_2/H_2 gas mixture at the reaction temperature, in order to ensure the complete reduction of the metallic species. The hydrodechlorination of $CF_3OCFClCF_2Cl$ was performed in a down-flow Hastelloy® tubular reactor equipped with an internal thermocouple. The reactor was inserted into an electric oven. A mixture of $CF_3OCFClCF_2Cl$, H_2 and N_2 was fed to the reactor. N_2 flow (inert) was calculated to obtain a feeding gas mixture containing 19% (v/v) $CF_3OCFClCF_2Cl$. The liquid $CF_3OCFClCF_2Cl$ reagent was introduced by a perfusion pump, then evaporated in a pre-heated mixer maintained at 80 °C. Catalytic tests were performed at 250 °C and 1 atm, with a 10-s contact time and $CF_3OCFClCF_2Cl/H_2$ molar ratio equal to 1. Tests took approximately 50 h. Reaction products were sampled after a water scrubber (HCl was the only restrained product) by an automatic looped-valve, and were analyzed by a TCD-equipped gas chromatograph.

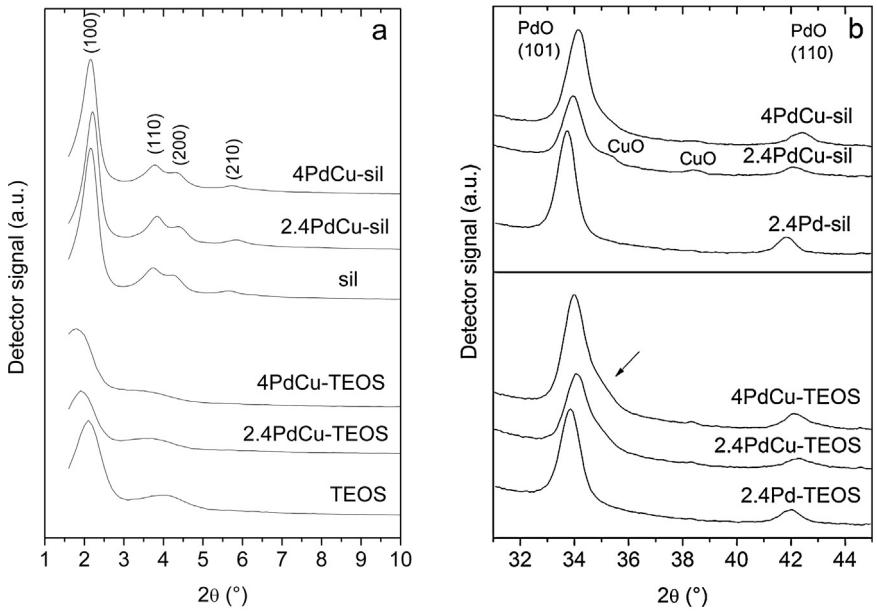

Fig. 1. Low angle diffraction patterns of bimetallic catalysts and MCM-41 materials (a) and wide angle diffraction patterns of mono- and bimetallic catalysts (b). The arrow indicates the shoulder due to a $Pd_{1-x}Cu_xO$ phase with a larger Cu content.

3. Results and discussion

3.1. Catalyst characterization

The chemical–physical characterization of samples was performed after the template removal by calcination at 540 °C and after activation in H_2.

XRD patterns in the low-angle region of calcined samples prepared from silicates and TEOS are shown in Fig. 1a. Diffraction patterns of silicate-derived samples display the (100), (110), (200), and (210) peaks of the hexagonal array of parallel mesopore cylinders. The addition of Cu and Pd metal precursors during the synthesis does not significantly alter the crystallinity of the MCM-41 structure as previously reported by us for low-loaded Pd/Cu samples [6]. Conversely, a broad peak due to the (100) plane and a bump in the 3–5 °2θ range are observed for TEOS-derived samples. Moreover, in these samples, peak positions are altered by the presence of copper and palladium cations. Reflections shift toward lower °2θ values with increases in the total metal content. This behavior has been previously associated with the inclusion of copper and palladium cations in the MCM-41 framework by Bálsamo et al. [31] and Papp et al. [34]. In the present work we observed that most of the Pd and Cu species during the template removal were present as oxides on the external surface of MCM-41 particles (see below).

Diffraction patterns of calcined samples were also recorded in the 31–45 °2θ range to study the formation of copper and/or palladium phases (Fig. 1b). Patterns of monometallic 2.4Pd-sil and 2.4Pd-TEOS samples display the (101) and (110) reflections of PdO at 33.7 and 41.9 °2θ, respectively. They are slightly shifted toward higher °2θ values in bimetallic catalysts due to the incorporation of Cu^{2+} into the PdO lattice; PdO and CuO may form homogeneous $Pd_{1-x}Cu_xO$ solid solutions up to an "x" value of 0.725 [43]. The asymmetric shape of the (101) peak indicates the presence of $Pd_{1-x}Cu_xO$ solid solutions with a different substitution degree. In particular, a shoulder at high °2θ is clearly observed for TEOS-derived samples, which may be ascribed to the inclusion of a large amount of Cu^{2+} in the PdO structure [43]. The total metal content does not appear to play a significant role in the type of crystalline phases formed with TEOS-derived samples, whereas it affects silicate-derived ones. Indeed, small amounts of segregated CuO are observed in the pattern of the 2.4PdCu-sil sample [44], while the (101) and (110) peaks are shifted toward higher values for the 4PdCu-sil sample.

These results seem to indicate that after the template removal by calcination at high temperature, most of the palladium and copper species are on the external surface of MCM-41 particles and form $Pd_{1-x}Cu_xO$ solid solutions whose composition mainly depends on the silica source. In particular, the copper content in $Pd_{1-x}Cu_xO$ is greater for TEOS-derived samples.

Specific surface area values and mesopore diameters are summarized in Table 1. S_{BET} values of pristine MCM-41 material prepared from silicates (sil) and 2.4PdCu-sil catalyst are similar (1164 and 1161 $m^2\,g^{-1}$, respectively). S_{BET} decreases slightly in the 4PdCu-sil catalyst (1002 $m^2\,g^{-1}$), which contains the highest total metal content. S_{BET} values are lower for TEOS-derived samples than those of silicate-derived ones. The metal loading seems to have a greater effect on the surface area, the S_{BET} value of the 4PdCu-TEOS is quite low (781 $m^2\,g^{-1}$). N_2 adsorption/desorption isotherms of pure MCM-41 materials and bimetallic catalysts, with the exception of 4PdCu-TEOS, are classified as Type IV (not shown), which is characteristic of MCM-41 mesoporous materials [45,46]. They show a steep capillary condensation step on uniform cylindrical mesopores in the 0.35–0.45 p/p^0 range which is followed by a plateau. Moreover, an adsorption at high p/p^0 values and a hysteresis loop above 0.4 p/p^0 are observed. These are related to the presence of secondary mesopores formed by the aggregation of particles. DFT pore size distribution curves display the expected peak in the 3.5–4.5 nm range with the maximum at around 4 nm (Table 1). In the isotherm of the 4PdCu-TEOS sample the adsorption due to ordered mesopores is lower and the plateau is not clearly observed. DFT analysis confirms that the total volume adsorbed in the 4.3 nm mesopores is lower in comparison to other samples, and that 6–7 nm pores are also present in this sample. The presence of large copper and palladium oxide particles may be responsible for the change in the sample textural properties [31,34].

Temperature programmed reduction profiles of mono- and bimetallic catalysts are shown in Fig. 2. Reduction profiles of monometallic palladium samples display a negative peak due to the decomposition of palladium hydride: the minimum of the peak is at around 90 and 77 °C for 2.4Pd-sil and 2.4Pd-TEOS, respectively. The

Table 1
Specific surface area (S_{BET}) and mesopore diameter (D_{meso}) values of silicate- and TEOS-derived supports and bimetallic catalysts.

	sil	2.4PdCu-sil	4PdCu-sil	TEOS	2.4PdCu-TEOS	4PdCu-TEOS
S_{BET} ($m^2\ g^{-1}$)	1164	1161	1002	1089	1008	781
D_{meso} (nm)	4.2	4.0	4.1	4.0	4.3	4.3

reduction of palladium may occur as soon as the sample is in contact with H_2, and it is not possible to measure it [47]. Reported results suggest that a lower amount of hydride is formed in TEOS-derived samples.

The shape of monometallic Cu catalyst profiles depends on the silica source. The 1.5Cu-TEOS profile displays a H_2 consumption peak with maximum at around 260 °C and two shoulders at lower temperatures (195 and 240 °C). Otherwise, two overlapping H_2 consumption peaks at around 236 and 310 °C are recorded for the 1.5Cu-sil sample. Larger copper particles in the silicate-derived sample than in the TEOS-derived one may explain the higher reduction temperatures [26].

Reduction profiles of bimetallic samples show a broad H_2 consumption peak for all the materials. The maxima of the H_2 consumption are recorded at 120–145 °C for silicate-derived samples and at 150–190 °C for TEOS-derived ones. The increase in the total metal loading only leads to a slight shift of the peak toward higher temperatures. The absence of the hydride decomposition peak for bimetallic samples may be related to the smaller size of Pd-Pd ensembles by Cu dilution. It is known that copper reduction can take place at lower temperatures in bimetallic catalysts, due either to H_2 spillover from Pd^0 to CuO [47–49] or to the formation of $Pd_{1-x}Cu_xO$ species [50]. The difference in reduction temperatures among silicate- and TEOS-derived samples may be explained by the Cu content in the $Pd_{1-x}Cu_xO$ mixed oxide as previously reported [51]. Indeed, diffraction data indicate that a larger amount of Cu is introduced in PdO for 2.4PdCu-TEOS and 4PdCu-TEOS samples, thus increasing the reduction temperature. However, the role of the particle size may not be ruled out.

Reduced catalysts were characterized by XRD, XPS, CO-DRIFTS, and HRTEM. The diffraction patterns of reduced samples in the 37–52°2θ range are displayed in Fig. 3. The patterns of monometallic 2.4Pd-sil and 2.4Pd-TEOS catalysts show the (111) and (200) diffraction lines of the face-centered-cubic (fcc) Pd metallic phase. Peak positions do not depend on the sample, but they are broader and less intense for 2.4Pd-TEOS, thus suggesting a lower crystallinity. In both silicate- and TEOS-derived samples, the presence of copper in catalysts makes the (111) and (200) reflections of Pd^0 shift toward higher °2θ values, confirming the replacement of Pd by smaller Cu atoms in disordered PdCu fcc alloys [52]. Moreover, peaks become less intense and broader, thus indicating the formation of smaller palladium/copper crystallites [17]. In the 2.4PdCu-sil sample, the (111) peak is actually made of two overlapping peaks at around 40.34 and 40.98°2θ, due to the formation of alloys with different Pd and Cu content. The cell parameters of the disordered fcc PdCu alloy were calculated: 0.388 nm for the 40.34°2θ, and 0.381 nm for the 40.98°2θ peaks; they are smaller than those obtained for the 2.4Pd-sil sample (0.389 nm). The amount of Pd in the alloys has been estimated to be 96 and 72 mol.%, assuming that PdCu solid solutions follow Vegard's law [15]. Two Pd-rich alloys have been also observed in the 4PdCu-sil sample, which contain around 94 and 73 mol.% Pd. However, the intensity of the peak at lower °2θ values decreases. In addition to reflections of the fcc PdCu alloy, a peak is clearly recorded at 43.10°2θ in silicate-derived catalysts. This has been attributed to the (110) reflection of the body-centered-cubic (bcc) β PdCu alloy previously observed in some catalysts [19,24,53,54], which coexists with the PdCu fcc phase [15,16]. A peak at around 78.06°2θ, due to the (211) peak of the bcc phase, is further evidence of its formation.

The diffraction patterns of TEOS-derived catalysts display two overlapping peaks at around 40.82 and 42.05°2θ. These may be attributed to fcc PdCu alloys with 78 mol% and 38 mol% Pd content. It would appear that the higher incorporation of Cu^{2+} into the PdO lattice which was observed in XRD patterns of calcined samples might be conducive to the inclusion of Cu in the fcc PdCu alloy during the reduction process. However, it should be stressed that the peak at around 42.05°2θ may be also attributed to the Cu_3Pd tetragonal phase, which has been observed for instance in $Pd/Cu–Al_2O_3$ catalysts [10].

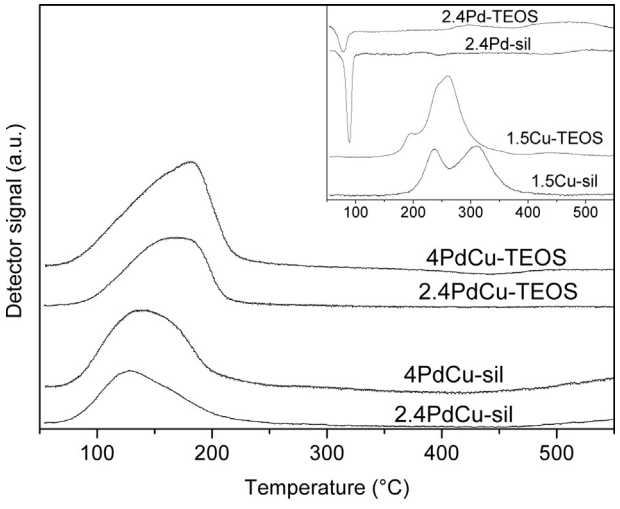

Fig. 2. TPR profiles of silicate- and TEOS-derived bimetallic and monometallic (inset) catalysts.

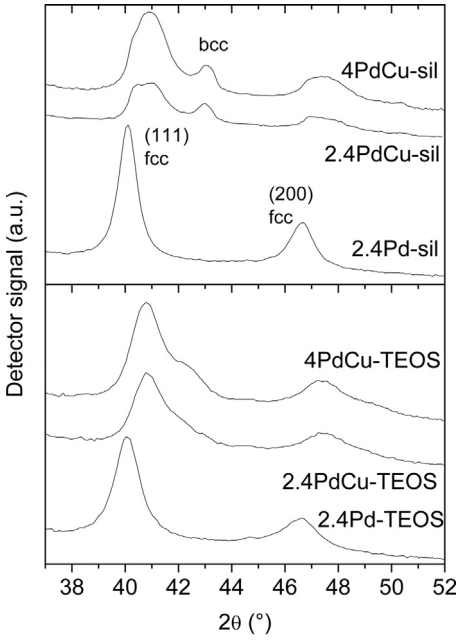

Fig. 3. XRD patterns in the 37–52°2θ range of reduced palladium-containing monometallic samples and bimetallic catalysts.

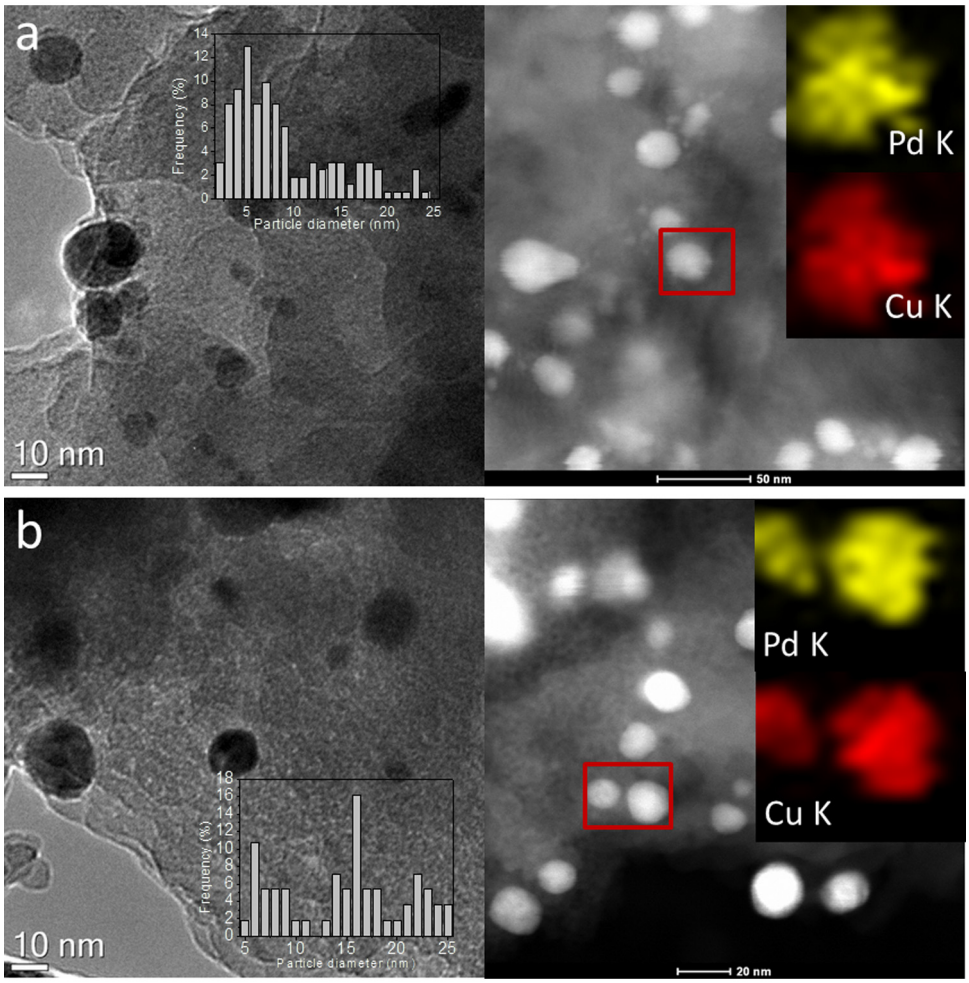

Fig. 4. HRTEM bright-field and STEM-HAADF images, STEM-EDS maps and particle size distribution histograms of reduced 4PdCu-sil (a) and 4PdCu-TEOS (b) catalysts.

Particle size distributions and compositions for all bimetallic catalysts were studied using HRTEM bright field images, STEM-HAADF images, and EDS line profiles and maps. Representative data of 4PdCu-sil and 4PdCu-TEOS samples are shown in Fig. 4. Spherical metallic particles are mainly present on the external surface of the MCM-41 support. A broad particle size distribution is observed, regardless of the silica source. For silicate-derived catalysts, the particle size increases as the total metal loading increases; it varies from 2 to 15 and 2 to 25 nm for 2.4PdCu-sil and 4PdCu-sil samples, respectively. Nevertheless, the average particle sizes do not change very much: they are centered at around 4 and 5 nm for 2.4 and 4 wt.% loaded samples. The formation of large particles may be related to the sintering that takes place during calcination. EDS maps and line profiles confirm the formation of bimetallic particles but copper and palladium content was not consistent, from particle to particle, in relation to the size. Indeed, it appears that smaller particles are mainly made of copper.

The average particle size increases in samples prepared from TEOS; likewise for silicate-derived catalysts, the higher the metal loading is, the larger the metallic particles are. In 2.4PdCu-TEOS samples, most of the particles are in the 7–20 nm range. The 4PdCu-TEOS catalyst contains three particle size distributions in the 5–11, 12–19, and 20–25 nm ranges. EDS analyses also confirm the presence of bimetallic particles in these materials.

Cu 2p and Pd 3d core-level XPS spectra of monometallic (2.4Pd-sil and 1.5Cu-sil) and 4 wt.% loaded bimetallic (4PdCu-sil and 4PdCu-TEOS) reduced catalysts were measured. XPS parameters are summarized in Table 2. In the Cu 2p core-level 1.5Cu-sil, 4PdCu-sil and 4PdCu-TEOS samples show a doublet corresponding to $2p_{3/2}$ and $2p_{1/2}$ orbitals. BEs values and the absence of bands corresponding to the characteristic satellites of Cu^{2+} indicate that copper is present as Cu^0 and/or Cu^+ [55,56]. In 1.5Cu-sil sample, the $2p_{3/2}$ peak is at 932.2 eV, with a FWHM of 3.5 and a spin–orbit coupling energy of 19.5 eV. XPS spectra of bimetallic

Table 2
XPS parameters of mono- and selected bimetallic catalysts.

Catalyst	BE (eV) Cu $2p_{3/2}$	FWHM (eV) Cu $2p_{3/2}$	BE (eV) Cu $2p_{1/2}$	FWHM (eV) Cu $2p_{1/2}$	BE (eV) Pd $3d_{5/2}$	FWHM (eV) Pd $3d_{5/2}$	BE (eV) Pd $3d_{3/2}$	FWHM (eV) Pd $3d_{3/2}$	Cu/Pd molar ratio
4PdCu-sil	931.8	3.6	951.3	3.6	335.1	2.8	340.3	2.8	1.30
4PdCu-TEOS	931.7	3.4	951.2	3.4	334.9	2.8	340.1	2.8	1.08
1.5Cu-sil	932.2	3.5	951.9	3.5					
2.4Pd-sil					335.0	2.0	340.2	2.0	

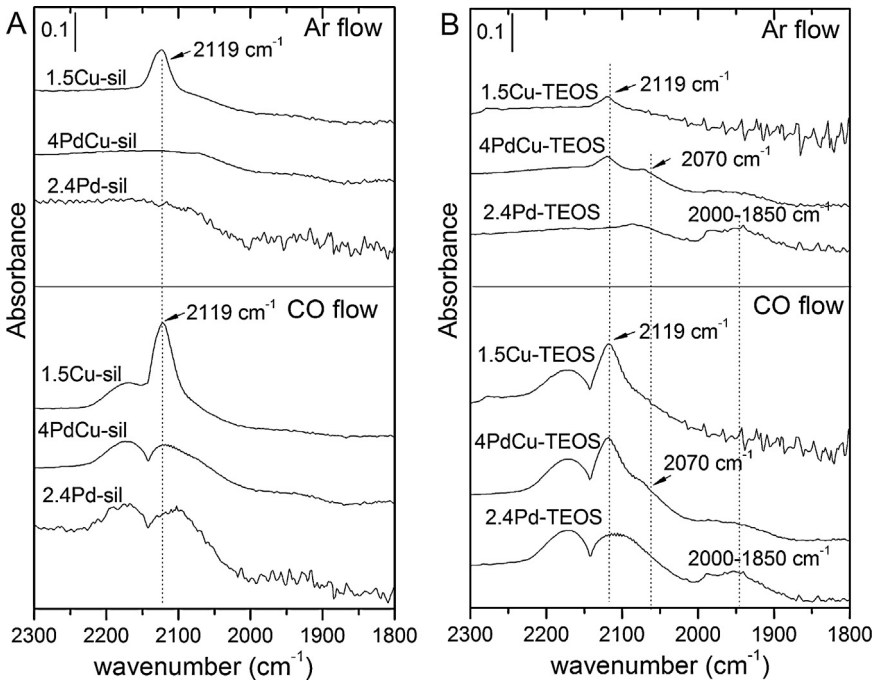

Fig. 5. Infrared spectra of CO adsorbed on selected reduced silicate-derived (A) and TEOS-derived (B) samples under CO and Ar flow.

particles evidence a shift in BE values toward lower eV and higher FWHM values that may be ascribed to the Pd–Cu interaction [17,20]. Pd 3d core-level XPS spectra of reduced catalysts show the characteristic doublet attributed to Pd $3d_{5/2}$ and Pd $3d_{3/2}$ in metallic palladium at 335.0–334.9 eV. No differences in BEs are observed among mono- and bimetallic catalysts, in agreement with previous results [17,48]; nevertheless, FWHM values are higher for bimetallic than for monometallic samples, a characteristic that may also be related to the Pd–Cu interaction [47]. Surface Cu/Pd atomic ratio values have been calculated for 4PdCu-sil and 4PdCu-TEOS samples (Table 2). The surface Cu/Pd molar ratio is 1.30 for 4PdCu-sil and 1.08 for 4PdCu-TEOS. The higher copper content in the surface of the silicate-derived sample might be related either to copper rich particles, as evidenced by HRTEM/EDS, or to the segregation of copper to the surface of bimetallic particles due to its higher mobility and lower surface energy [8]. Moreover, it should be considered that, depending on the crystalline phase present on the surface, the amount of exposed Cu atoms may change, thus affecting the measured Cu/Pd ratio [19].

Fig. 5A and B show CO-DRIFTS spectra under CO and Ar flow, at room temperature, on monometallic samples and bimetallic reduced catalysts at the highest metal content (4PdCu-sil and 4PdCu-TEOS). The spectra of all the samples under CO atmosphere show the typical IR bands at 2175 and 2115 cm^{-1}, corresponding to the maxima in the vibration-rotational spectrum of gaseous CO [57,58]. The presence/absence of IR bands due to the interaction of CO with palladium and copper species under CO atmosphere and their evolution after Ar and heat treatment depend on the studied samples.

No bands caused by the interaction between Pd and CO are observed in Pd silicate-derived samples, whereas, in the 2.4Pd-TEOS spectrum, weak bands at 2000–1850 cm^{-1} can be seen. These bands may be attributed to the bridged CO species adsorbed on the Pd^0 surface. After the removal of CO by Ar stream, these bands are preserved after heating at 150 °C (not shown).

In the spectra under CO flow of Cu-containing samples, in addition to IR bands of gaseous CO, an additional band is recorded at 2119 cm^{-1}, regardless of the silica source. This new band corresponds to the linear adsorption of CO on oxidized Cu particles, mainly on Cu^+ species [59–61]. The CO–Cu^+ band persists after Ar flow and heating at 50 °C and is more intense for the 1.5Cu-sil sample, thus indicating a higher amount of oxidized Cu^+ species on the surface of this catalyst.

The presence of copper modifies the adsorption of CO in bimetallic catalysts. The spectrum of the 4PdCu-sil sample after CO removal shows a very weak and broad band between 2000 and 1850 cm^{-1} due to bridged adsorption of CO on a few Pd^0 sites [25]. The CO–Cu^+ band observed in the monometallic Cu-sil sample is absent in bimetallic catalysts despite the large copper content in their surface revealed by XPS. Conversely, in 4PdCu-TEOS material, bands owing to both CO–Pd^0 and CO–Cu^+ interactions are recorded under CO atmosphere and after Ar and heat treatment. These bands may be assigned to: (i) linear adsorption of CO on Cu^+ (2119 cm^{-1}); (ii)

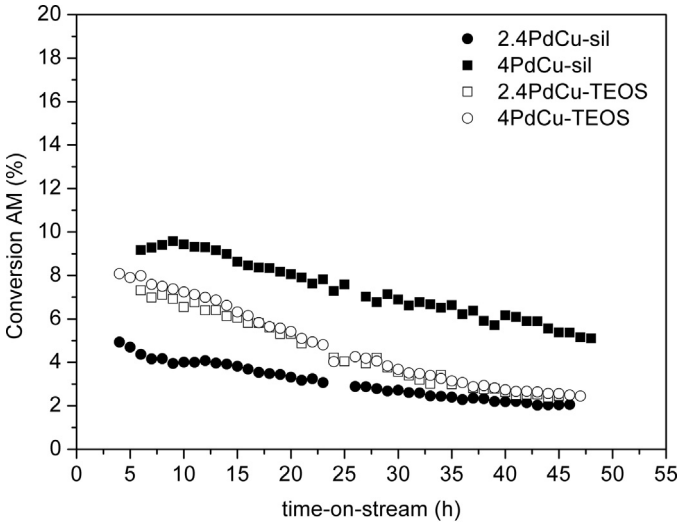

Fig. 6. Evolution in the conversion of $CF_3OCFClCF_2Cl$ (AM) with time-on-stream for bimetallic silicate-derived and TEOS-derived catalysts.

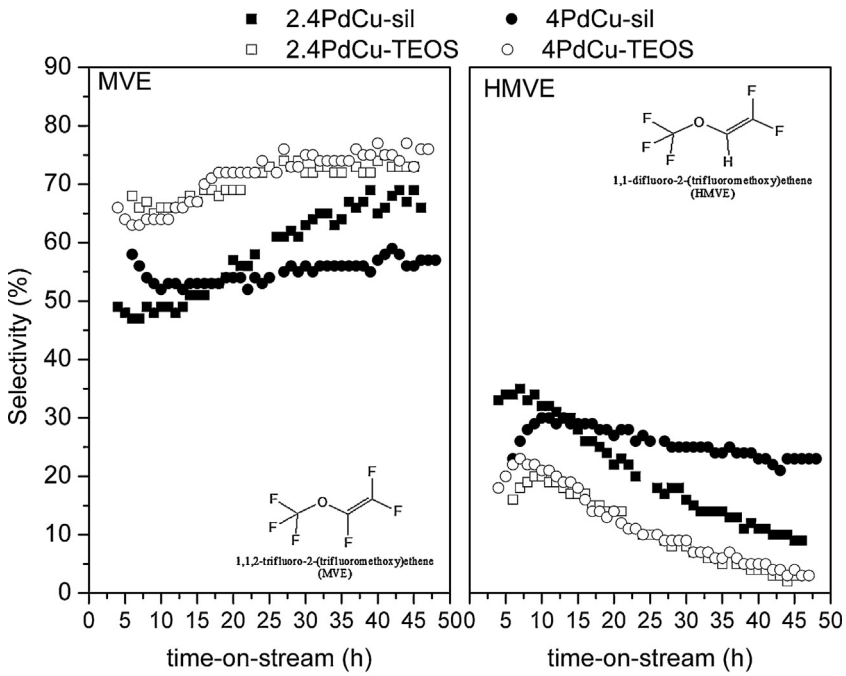

Fig. 7. Selectivity in $CF_3OCF{=}CF_2$, MVE (a) and $CF_3OCH{=}CF_2$, HMVE (b) for bimetallic silicate-derived and TEOS-derived catalysts.

bridged adsorption of CO on metallic Pd (2000–1850 cm^{-1}); iii) linear adsorption of CO on Pd^0 (sh 2070 cm^{-1}) [49,62]. These bands are stable after CO desorption at 50 °C.

The changes in the spectra after the introduction of Cu may be explained by an ensemble effect: namely, Cu "dilutes" palladium particles [13,25,49,63,64]. Thus, in bimetallic TEOS-derived samples, copper decreases the amount of bridged CO–Pd^0 adsorbed on large particles and, therefore, increases the amount of linear CO–Pd^0 species [8], while in the less dispersed silicate-derived samples, the presence of copper makes it possible to see only the bridged Pd^0–CO species.

3.2. Catalytic activity

The evolution in the conversion of $CF_3OCFClCF_2Cl$ (AM) with time-on-stream over all the bimetallic catalysts is shown in Fig. 6. For silicate-derived catalysts, the conversion increases when increasing the metal loading from 5% over 2.4PdCu-sil to 10% over 4PdCu-sil. Nevertheless, a continuous deactivation is observed for both catalysts. Conversely, no differences were observed in the conversion when increasing the metal content by using TEOS-derived catalysts. Regardless of the silica source or metal loading, the main reaction product was the target unsaturated dechlorinated compound, $CF_3OCF{=}CF_2$ (MVE), while the primary by-products were the unsaturated $CF_3OCH{=}CF_2$ (HMVE), the hydrogenated $CF_3OCFClCHF_2$ (AMH), and the Cl–F exchanged $CF_3OCCl{=}CF_2$ compounds.

The selectivities to $CF_3OCF{=}CF_2$ and $CF_3OCH{=}CF_2$ are shown in Fig. 7. The formation of the target $CF_3OCF{=}CF_2$ compound was more significant with TEOS-derived catalysts and, as with conversion values, no notable differences have been found depending on the total metal loading. A slight decrease in selectivity to $CF_3OCF{=}CF_2$ was observed during the first 10 h of time-on-stream, and then it steadily increased. Selectivity values of 73 and 76% were reached at 50 h reaction time with 2.4PdCu-TEOS and 4PdCu-TEOS, respectively. With 2.4PdCu-sil the selectivity followed the same trend as with TEOS-derived catalysts, and after 50 h reaction the MVE selectivity was 66%. Conversely, with the high-loaded 4PdCu-sil catalyst, the decrease in the formation of $CF_3OCF{=}CF_2$ was rather important during the first 10 h time-on-stream, after which its production rate did not vary significantly. The selectivity to HMVE roughly followed a trend opposite to that of MVE, thus suggesting a connection in the formation of these two molecules.

Selectivities to $CF_3OCClFCHF_2$ and $CF_3OCCl{=}CF_2$ (not shown) are below 8% regardless of the metal loading and silica source. The formation of the saturated $CF_3OCClFCHF_2$ compound decreased during the first 10–15 h reaction time, after which its production was almost constant. The hydrogenating activity of silicate-derived catalysts, especially of 2.4PdCu-sil, was higher than those of TEOS-derived ones.

It is known that size and composition of metallic particles are the main features that determine the activity, selectivity, and deactivation process over metallic supported catalysts [4,7,13]. Indeed, the higher conversion achieved with the 4PdCu-sil catalyst may be related to the higher metal loading and smaller particles present over this sample. Palladium monometallic catalyst produces large quantities of the $CF_3OCClFCHF_2$ hydrogenated product and the catalyst deactivates quickly [7]. On the other hand, the monometallic Cu catalyst is not active because of its rapid deactivation due to chlorine poisoning [7]. For bimetallic catalysts, their selectivity is related to the palladium and copper content in the alloy particles. In silicate-derived catalysts, the presence of some palladium-enriched alloys detected by XRD may promote the formation of AMH and the F/H substitution to produce HMVE. Copper-rich particles may quickly deactivate with time-on-stream. On the other hand, the higher copper content in the PdCu alloys obtained from TEOS-derived samples may lead to the combination of sites for dechlorination, keeping under control the activation of H_2 from Pd to clean the surface of the catalyst.

4. Conclusions

Chemical/physical and catalytic properties of Pd/Cu-MCM-41 for the hydrodechlorination of $CF_3OCFClCF_2Cl$ to $CF_3OCF{=}CF_2$ were shown to depend mainly on the silica source (silicate and TEOS) used for catalyst preparation, while they were not significantly influenced by the total metal loading. The MCM-41 structure was not affected by the addition of Pd and Cu during the synthesis,

with the exception of the high-loaded TEOS-derived sample. The calcination treatment, to remove the template, led to the formation of palladium and copper as $Pd_{1-x}Cu_xO$ oxides on the external surface of MCM-41 particles. The properties and composition of the $Pd_{1-x}Cu_xO$ solid solution were shown to influence the properties of the metallic particles obtained by H_2 reduction. The broad size distribution of large metallic particles is mainly related to the sintering taking place primarily during calcination. The size of the metallic particles increases as the metal content increases, while their composition depends on the silica source. Palladium- and copper-rich particles in silicate-derived samples may decrease the selectivity to the target dechlorinated unsaturated product. The incorporation of a higher amount of Cu^{2+} in $Pd_{1-x}Cu_xO$ for TEOS-derived samples leads to an increase in the reduction temperature and fosters the incorporation of more Cu into the fcc PdCu alloy. The combination of Cu sites for dechlorination, and Pd sites with a tailored activity to activate H_2 and clean the catalyst surface, may explain the higher selectivity in the unsaturated product for TEOS-derived samples.

Acknowledgments

INSTM (Consorzio Interuniversitario Nazionale per la Scienza e Tecnologia dei Materiali - Italy) is acknowledged for co-financing the PhD project of Manuel Gregori. Authors also thank the Universidad Nacional del Litoral (UNL- Argentina), Consejo Nacional de Investigaciones Científicas y Técnicas (CONICET - Argentina), and ANPCyT SPECS (PME8-2003) for their financial support.

References

[1] D.A. Babb, G. Hougam, P.E. Cassidy, K. Johns, T. Davidson, Fluoropolymers 1. Synthesis, Kluwer Academic Pub., New York, 2002, pp. 34–35.
[2] V. Tortelli, P. Calini, A. Zompatori, E. Antenucci, Patent US 203368 assigned to Solvay Solexis Spa (Italy) (2007).
[3] S. Albonetti, M. Gregori, G. Fornasari, S. Millefanti, V. Tortelli, G. Marchionne, Patent WO/104365 assigned to Solvay Specialty Polymers Italy SpA (2012).
[4] M. Gregori, G. Fornasari, G. Marchionni, V. Tortelli, S. Millefanti, S. Albonetti, Appl. Catal. A: Gen. 470 (2014) 123–131.
[5] S. El Mourabit, M. Guillot, G. Toquer, J. Cambedouzou, F. Goettmann, A. Grandjean, RSC Adv. 2 (2012) 10916–10924.
[6] M. Gregori, P. Benito, G. Fornasari, M. Migani, S. Millefanti, F. Ospitali, S. Albonetti, Microporous Mesoporous Mater. 190 (2014) 1–9.
[7] P. Benito, M. Gregori, S. Andreoli, G. Fornasari, S. Millefanti, F. Ospitali, S. Albonetti, Catal. Today (2014), http://dx.doi.org/10.1016/j.cattod.2014.01.034.
[8] S. Lambert, B. Heinrichs, A. Brasseur, A. Rulmont, J.P. Pirard, Appl. Catal. A: Gen. 270 (2004) 201–208.
[9] S. Lambert, F. Ferauche, A. Brasseur, J.-P. Pirard, B. Heinrichs, Catal. Today 100 (2005) 283–289.
[10] N. Barrabés, D. Cornado, K. Foettinger, A. Dafinov, J. Llorca, F. Medina, G. Rupprechter, J. Catal. 263 (2009) 239–246.
[11] A. Śrębowata, W. Lisowski, J.W. Sobczak, Z. Karpiński, Catal. Today 175 (2011) 576–584.
[12] M.A. Keane, ChemCatChem 3 (2011) 800–821.
[13] B.T. Meshesha, N. Barrabés, J. Llorca, A. Dafinov, F. Medina, K. Föttinger, Appl. Catal. A: Gen. 453 (2013) 130–141.
[14] M. Bonarowska, O. Machynskyy, D. Łomot, E. Kemnitz, Z. Karpiński, Catal. Today (2014), http://dx.doi.org/10.1016/j.cattod.2014.01.029.
[15] P.R. Subramanian, D.E. Laughlin, J. Phase Equilib. 12 (1991) 231–243.
[16] S.M. Opalka, W. Huang, D. Wang, T.B. Flanagan, O.M. Løvvikd, S.C. Emerson, Y. She, T.H. Vanderspurt, J. Alloys Compd. 446–447 (2007) 583–587.
[17] B.L. Gustafson, P.S. Wehner, Appl. Surf. Sci. 52 (1991) 261–270.
[18] F. Skoda, M.P. Astier, G.M. Pajonk, M. Primet, Catal. Lett. 29 (1994) 159–168.
[19] A. Renouprez, K. Lebas, G. Bergeret, J. Mol. Catal. A: Chem. 120 (1997) 217–225.
[20] A.M. Venezia, L.F. Liotta, G. Deganello, Z. Schay, L. Gucziz, J. Catal. 182 (1999) 449–455.
[21] K. Sun, J. Liu, N.K. Nag, N.D. Browning, J. Phys. Chem. B 106 (2002) 12239–12246.
[22] J. Sá, H. Vinek, Appl. Catal. B: Environ. 57 (2005) 247–256.
[23] O.S.G.P. Soares, J.J.M. Órfão, J. Ruiz-Martínez, J. Silvestre-Albero, A. Sepúlveda-Escribano, M.F.R. Pereira, Chem. Eng. J. 165 (2010) 78–88.
[24] M. Bonarowska, W. Juszczyk, Z. Karpiński, J. Catal. 301 (2013) 112–115.
[25] M. Fernández-García, J.A. Anderson, G.L. Haller, J. Phys. Chem. 100 (1996) 16247–16254.
[26] M. Hartmann, S. Racouchot, C. Bischof, Microporous Mesoporous Mater. 27 (1999) 309–320.
[27] G. Zhang, J. Long, X. Wang, Z. Zhang, W. Dai, P. Liu, Z. Li, L. Wu, X. Fu, Langmuir 26 (2010) 1362–1371.
[28] S. Velu, L. Wang, M. Okazaki, K. Suzuki, S. Tomura, Microporous Mesoporous Mater. 54 (2002) 113–126.
[29] M. Ziolek, I. Nowak, B. Kilos, I. Sobczak, P. Decyk, M. Trejda, J.C. Volta, J. Phys. Chem. Solids 65 (2004) 571–581.
[30] C.M. Chanquia, L. Andrini, J.D. Fernandez, M.E. Crivello, F.G. Requejo, E.R. Herrero, G.A. Eimer, J. Phys. Chem. A 114 (2010) 12221–12229.
[31] N.F. Bálsamo, C.M. Chanquía, E.R. Herrero, S.G. Casuscelli, M.E. Crivello, G.A. Eimer, Ind. Eng. Chem. Res. 49 (2010) 12365–12370.
[32] M. Li, K.N. Hui, K.S. Hui, S.K. Lee, Y.R. Cho, H. Lee, W. Zhou, S. Cho, C.Y.H. Chao, Y. Li, Appl. Catal. B: Environ. 107 (2011) 245–252.
[33] J. Panpranot, K. Pattamakomsan, P. Praserthdam, J.G. Goodwin Jr., Ind. Eng. Chem. Res. 43 (2004) 6014–6020.
[34] A. Papp, A. Molnár, A. Mastalir, Appl. Catal. A: Gen. 289 (2005) 256–266.
[35] C. Sener, T. Dogu, G. Dogu, Microporous Mesoporous Mater. 94 (2006) 89–98.
[36] D. Lee, G.S. Jung, H.C. Lee, J.S. Lee, Catal. Today 111 (2006) 373–378.
[37] A. Mastalir, B. Rác, Z. Király, A. Molnár, J. Mol. Catal. A: Chem. 264 (2007) 170–178.
[38] S. Domínguez-Domínguez, Á. Berenguer-Murcia, Á. Linares-Solano, D. Cazorla-Amorós, J. Catal. 257 (2008) 87–95.
[39] S.-H. Chung, Y.-M. Park, M.-S. Kim, K.-Y. Lee, Catal. Today 185 (2012) 205–210.
[40] J.S. Beck, J.C. Vartuli, W.J. Roth, M.E. Leonowicz, C.T. Kresge, K.D. Schmitt, C.T.-W. Chu, D.H. Olson, E.W. Sheppard, S.B. McCullen, J.B. Higgins, J.L. Schlenker, J. Am. Chem. Soc. 114 (1992) 10834–10843.
[41] K. Cassiers, T. Linssen, M. Mathieu, M. Benjelloun, K. Schrijnemakers, P. Van Der Voort, P. Cool, E.F. Vansant, Chem. Mater. 14 (2002) 2317–2324.
[42] M.A. Álvarez-Montero, L.M. Gómez-Sainero, J. Juan-Juan, A. Linares-Solano, J.J. Rodriguez, Chem. Eng. J. 162 (2010) 599.
[43] G.L. Christensen, M.A. Langell, J. Phys. Chem. C 117 (2013) 7039–7049.
[44] C.-M. Niu, P.H. Rieger, K. Dwight, A. Wold, J. Solid State Chem. 86 (1990) 175–179.
[45] M. Kruk, M. Jaroniec, Langmuir 13 (1997) 6267–6273.
[46] M. Kruk, M. Jaroniec, Y. Yang, A. Sayari, J. Phys. Chem. B 104 (2000) 1581–1589.
[47] P. Reyes, A. Figueroa, G. Pecchi, J.L.G. Fierro, Catal. Today 62 (2000) 209–217.
[48] J. Jung, S. Bae, W. Lee, Appl. Catal. B: Environ. 127 (2012) 148–158.
[49] S. Sitthis, T. Pham, T. Prasomsri, T. Sooknoi, R.G. Mallinson, D.E. Resasco, J. Catal. 280 (2011) 17–27.
[50] J. Batista, A. Pintar, D. Mandrino, M. Jenko, V. Martin, Appl. Catal. A: Gen. 206 (2001) 113–124.
[51] Z. Xu, L. Chen, Y. Shao, D. Yin, S. Zheng, Ind. Eng. Chem. Res. 48 (2009) 8356–8363.
[52] A. Anastasopoulos, L. Hannah, B.E. Hayden, J. Catal. 305 (2013) 27–35.
[53] N.N. Kariuki, X. Wang, J.R. Mawdsley, M.S. Ferrandon, S.G. Niyogi, J.T. Vaughey, D.J. Myers, Chem. Mater. 22 (2010) 4144–4152.
[54] V. Sanchez-Escribano, L. Arrighi, P. Riani, R. Marazza, G. Busca, Langmuir 22 (2006) 9214–9219.
[55] M.A. Álvarez-Montero, L.M. Gómez-Sainero, J. Juan-Juan, A. Linares-Solano, J.J. Rodriguez, Chem. Eng. J. 162 (2010) 599–608.
[56] E.B. Fox, S. Velu, M.H. Engelhard, Y.-H. Chin, J.T. Miller, J. Kropf, C. Song, J. Catal. 260 (2008) 358–370.
[57] C. Vignatti, M.S. Avila, C.R. Apesteguía, T.F. Garetto, Int. J. Hydrogen Energy 35 (2010) 7302–7312.
[58] D. Liu, G.H. Que, Z.X. Wang, Z.F. Yan, Catal. Today 68 (2001) 155–160.
[59] K.I. Choi, M.A. Vannice, J. Catal. 131 (1991) 36–50.
[60] A. Marchi, Trends Appl. Spectrosc. 4 (2002) 239–251.
[61] J. Pritchard, T. Catterick, R.K. Gupta, Surf. Sci. 53 (1975) 1–20.
[62] M. Primet, M.V. Mathieu, W.M.H. Sachtler, J. Catal. 4 (1976) 324–327.
[63] V. Ponec, Appl. Catal. A: Gen. 222 (2001) 31–45.
[64] E. Jeroro, M.P. Hyman, J.M. Vohs, Phys. Chem. Chem. Phys. 11 (2009) 10457–10465.